Characterization of FeCo−SiO_2 Nanocomposite Films Prepared by Sol−Gel Dip Coating

M. F. Casula and A. Corrias*

Dipartimento di Scienze Chimiche, Università di Cagliari, Cittadella Universitaria, S.S. 554 bivio per Sestu, 09042 Monserrato (Cagliari), Italy

A. Falqui and V. Serin

CEMES/CNRS, 29 Rue Jeanne Marvig, 31055 Toulouse, France

D. Gatteschi and C. Sangregorio

Dipartimento di Chimica, Università di Firenze, Via della Lastruccia 3, 50019 Sesto Fiorentino (Firenze), Italy

C. de Julián Fernández

INFM, Dipartimento di Fisica Galileo Galilei, Università di Padova, Via Marzolo 8, 35131 Padova, Italy

G. Battaglin

INFM, Dipartimento di Chimica Fisica, Università di Venezia, Calle larga Santa Marta 2137, 30123 Venezia, Italy

Received December 4, 2002. Revised Manuscript Received March 24, 2003

FeCo−SiO_2 nanocomposite films on silica glass substrates were prepared by the sol−gel method and characterized by X-ray diffraction, transmission electron microscopy, Rutherford backscattering spectrometry, extended X-ray absorption fine structure spectroscopy, and magnetic susceptibility measurements. FeCo alloy nanoparticles with average sizes around 10 nm were obtained which are well dispersed in the silica matrix and show superparamagnetic behavior. The experimental conditions of the sol−gel preparation influence the thickness and homogeneity of the films. The magnetic properties are also affected by preparation conditions.

1. Introduction

Metal−insulator nanocomposites have attractive optical, magnetic, and transport properties which make them candidates for use in several micro- and nanodevices.[1] These composites are often constituted by noble metal or transition metal particles, with sizes in the 1−15 nm range, dispersed in a dielectric matrix. From the standpoint of the magnetic properties these nanoparticles are single domain[2] and often exhibit unusual properties such as superparamagnetic behavior,[3,4] enhanced magnetic moment,[5] enhanced coercivity,[4] spin glass behavior[6,7] and exchange coupling effects.[8,9] The size effects, that is the modification of electronic, structural, and magnetic properties due to the reduced dimension of the particles and the increased magnetic contribution of surface atoms, are responsible for these properties.[10]

Most of the studies have been devoted to nanocomposites containing single metal nanoparticles; only recently has the attention turned to bimetallic composites as well. In principle, the preparation of such systems could allow tailoring of the magnetic properties by varying almost continuously the composition, as it is well-known that the alloys have peculiar magnetic properties different from those of single-metal-based materials. For example, in the past few years the research has mainly focused on the preparation and study of FePt and CoPt based composites because of their very large magnetic anisotropy.[11,12]

* To whom correspondence should be addressed. Tel: +39 070 6754351. Fax: +39 070 6754388. E-mail: corrias@unica.it.

(1) Singh Nalwa, H., Ed. *Handbook of Nanostructured Materials and Nanotechnology*; Academic Press: San Diego, CA, 2000.
(2) Néel, L. *Ann. Geophys.* **1949**, *5*, 99.
(3) Dormann, J. L.; Fiorani, D.; Tronc, E. *Adv. Chem. Phys.* **1997**, *98*, 283.
(4) Chien, C. L. In *Science and Technology of Nanostructures Magnetic Materials;* Hadjipanayis, G., Prinz, G. A., Eds.; Plenum Press: New York, 1991; Vol. 259, p 477.
(5) Billas, I. M. L.; Châtelain, A.; de Heer, W. A. *Science* **1994**, *265*, 1682.
(6) Luo, W.; Nagel, S. R.; Rosenbaum, T. F.; Rosenzweig, R. E. *Phys. Rev. Lett.* **1991**, *67*, 2121.
(7) Dormann, J. L.; Chekaoui, R.; Spinu, L.; Nogues, M.; Lucari, F.; D'Orazio, F.; Fiorani, D.; Garcia, A.; Tronc, E.; Jolivet, J. P. *J. Magn. Magn. Mater.* **1998**, *187*, L139.
(8) Kodama R.; Berkovitz, A. E. *Phys. Rev. B* **1999**, *59*, 6321.
(9) Gangopadhyay, S.; Hadjipanayis, G.; Sorensen, C. M.; Klabunde, K. J. *Nanostructured Materials*; Pergamon Press: Oxford, 1992; Vol. 1, p 449.
(10) Kodama, R. H. *J. Magn. Magn. Mater.* **1999**, *200*, 359.

10.1021/cm0217755 CCC: $25.00
Published on Web 04/25/2003

Magnetic nanoparticles have been considered especially attractive for applications in data storage which requires materials with large coercivity, remanence, and time stability at room temperature. However, other kinds of applications are now devised for nanocomposite materials. For example, nanocomposites with soft magnetic properties can be incorporated in high-frequency devices and in micro-transductors which require large magnetic moment and susceptibility, low coercivity, and large resistivity.[13−15] Recently, several groups have studied the magnetic and high-frequency properties of FeCo nanocomposites films with different insulator matrixes.[16−18] For example, FeCo−Al_2O_3 films have been included in a 300 MHz spiral-shaped inductor prototype.[18] Moreover the magneto-transport properties of these composites have been investigated,[18−20] showing up to 10% magnetoresistance at room temperature.[18]

From the standpoint of micro and nano applications, preparation of composites in the form of thin films is highly desirable. The sol−gel method is well suited for the preparation of films because the fluid properties of the sol prior to gelation allow spin-, dip-, or spray-coating. Moreover, compared to conventional thin-film forming processes such as CVD, evaporation or sputtering, sol−gel thin-film formation requires considerably less equipment and is less expensive.[21] In particular, the easiest coating procedure is provided by dip-coating, although this technique is suitable only if all the substrate has to be coated. Sol−gel films preparation routes have been developed for the production of protective and antireflection coatings[22] and for optical sensor application.[23] In the field of nanocomposites, copper, silver, and gold−silica films have been studied mainly because of their large third-order optical nonlinearity,[24,25] although the preparation of different metals dispersed on pure or modified silica by the sol−gel method has also been shown to be successful.[26,27] Several studies on CoNi alloy−silica nanocomposites films prepared by sol−gel have been realized with the aim of studying the optical and magnetic properties;[28,29] however, the studies on these materials are still largely unexplored.

Recently, the synthesis of FeCo−SiO_2 nanocomposites in the form of xerogels[30] and aerogels[31] has been carried out. In this paper the study is extended to the synthesis of FeCo−SiO_2 thin films using a sol−gel dip-coating procedure on silica glass substrates. The effect of the coating process on the structure, morphology, and magnetic properties of the alloy particles is discussed. Because the characteristics of the film can depend on reactions between the sol and the silanol groups at the surface of the silica glass substrate[32] the effect of pretreatment of the substrate is also studied.

2. Experimental Section

The sol was prepared using tetraethoxysilane (TEOS, 98% Aldrich) as silica precursor and Fe(II) and Co(II) acetates (Fe-$(CH_3COO)_2$ and $Co(CH_3COO)_2{\cdot}4H_2O$) as metal precursors. The total metal content in the final composite was 10 wt % (Fe + Co/(Fe + Co + SiO_2)) and the iron-to-cobalt ratio was equal to 1. An ethanolic solution of TEOS was added dropwise to an hydroethanolic solution of the iron and cobalt acetates, which were dissolved by adding glacial acetic acid. After stirring for 1 h, a clear sol was obtained, having pH = 3.8 and Si/H_2O/EtOH molar ratio equal to 1:4:19. The sol, having an initial volume of 97 mL, was poured into the Teflon vessel of the dipping apparatus, so that the initial surface-to-volume ratio was 0.12. Under these conditions the sol would gelate in about 20 days. The dipping was performed either on the unaged sol or after aging for a few days. Because of the slow gelation, it is likely that the sol does not undergo a strong increase in viscosity and density during the first days of sol aging. The dipping was performed by a motor-driven dipper with a speed of 3.3 mm·s^{-1} using 75 × 25 × 1 mm silica glass substrates (Heraeus, Herasil I). Prior to dipping, the substrate was cleaned using hot solfochromic mixture, rinsed with distilled water and ethanol, and then stored in a desiccator. Because it is known that a strong base can modify the silica surface, the effect of a pretreatment of the substrate with a 0.1 M solution of potassium hydroxide on the adhesion of the film was tested.

The multiple dipping technique was used. After each dip, the films were dried at 50 °C in static air. After the last dip they were thermally treated at 350 °C for 1 h in static air and finally reduced at 800 °C for 2 h under flowing hydrogen (80 mL·min^{-1}). The reduction treatment was performed in a tubular quartz reactor with a rotating sample holder to ensure homogeneous heating conditions.

At all stages the films were stored in a desiccator since it has been reported that humidity may induce modifications such as further hydrolysis affecting the film thickness.[23] In Table 1 the acronyms and the preparation details of the film samples which were submitted to further investigation are reported.

XRD spectra were collected on a Seifert ×3000 diffractometer equipped with a grazing incidence attachment (GID), a graphite monochromator, and Cu Kα radiation.

(11) Sun, S.; Murray, C. B.; Weller, D.; Folks, L.; Moser, A. *Science* **2000**, *287*, 1989.
(12) Christodoulides, J. A.; Zhang, Y.; Hadjipanayis, G. C.; Fountzoulas, C. *IEEE Trans. Magn.* **2000**, *36*, 2333.
(13) Ohnuma, S.; Lee, H. J.; Kobayashi, N.; Fujimori, H.; Masumoto, T. *IEEE Trans. Magn.* **2001**, *37*, 2251.
(14) Russek, S.; Kabois, P.; Silva, T.; Mancoff, F. B.; Wang, S. D.; Qian Z.; Daughton, J. M. *IEEE Trans. Magn.* **2001**, *37*, 2248.
(15) Ohnuma, S.; Masumoto, T. *Acta Mater.* **2001**, *44*, 1309.
(16) Ohnuma, S.; Kobayashi, N.; Masumoto, T.; Mitami, S.; Fujimori, H. *J. Appl. Phys.* **1999**, *85*, 4543.
(17) Ikeda K.; Kobayashi, N.; Fujimori, H. *J. Appl. Phys.* **2002**, *92*, 5395.
(18) Vovk, A. Ya.; Wang, J. Q.; Pogoriliy, A. M.; Shypil, O. V.; Kravets A. F.; *J. Magn. Magn. Mater.* **2002**, *242−245*, 476.
(19) Kakazei, G. N.; Pogorelov, Yu. G.; Lopes, A. M. L.; Sousa, J. B.; Cardoso, S.; Freitas, P. P.; Pereira de Azevedo, M. M.; Snoeck, E. *J. Appl. Phys.* **2001**, *90*, 4144.
(20) Kobayashi, N.; Ohnuma, S.; Masumoto, T.; Fujimori, H. *J. Appl. Phys.* **2001**, *90*, 4159.
(21) Brinker, C. J.; Scherer, G. W. *Sol−Gel Science*; Academic Press: San Diego, CA, 1990; Chapter 13.
(22) Floch, H. G.; Belleville, P. F. *J. Sol-Gel Sci. Technol.* **1994**, *1*, 293.
(23) McDonagh, C.; Sheridan, F.; Butler, T.; MacCraith, B. D. *J. Non-Cryst. Solids* **1996**, 194, 72.
(24) De, G.; Licciulli, A.; Massaro, C.; Tapfer, L.; Catalano, M.; Battaglin, G.; Meneghini C.; Mazzoldi, P. *J. Non-Cryst. Solids* **1996**, *194*, 225.
(25) Yonezawa, T.; Matsune, H.; Kunitake, T. *Chem. Mater.* **1999**, *11*, 33.
(26) Chatterjee, A.; Chakravorty, D. *J. Phys. D* **1990**, *23*, 1097.
(27) Prokopenko, V. B.; Gurin, V. S.; Alexeenko, A. A.; Kulikauskas V. S.; Kovalenko, D. L. *J. Phys. D* **2000**, *33*, 3152.
(28) de Julián Fernández, C.; Sangregorio, C.; Mattei, De, G. Saber, A.; Lo Russo, S.; Battaglin, G.; Catalano, M.; Cattaruzza, E.; Gonella, F.; Gatteschi, D.; Mazzoldi, P. *Mater. Sci. Eng. C* **2001**, *15*, 59.
(29) Mattei, G.; de Julián Fernandez, C.; Mazzoldi, P.; Sada, C.; De, G.; Battaglin, G.; Sangregorio, C.; Gatteschi, D. *Chem. Mater.* **2002**, *14*, 3440.
(30) Ennas, G.; Casula, M. F.; Falqui, A.; Gatteschi, D.; Marongiu, G.; Piccaluga, G.; Sangregorio, C.; Pinna, G. *J. Non-Cryst. Solids* **2001**, *293−295*, 1.
(31) Casula, M. F.; Corrias, A.; Paschina, G. *J. Mater. Chem.* **2002**, *12*, 1505.
(32) Bel Hadj, F.; Sampere, R.; Phalippou, J. *J. Non-Cryst. Solids* **1986**, *2*, 417.

Table 1. Acronyms of the Samples and Sol−Gel Preparation Conditions

	sol aging	pretreatment of the substrate with KOH	number of dips
F1	3 days	no	1
F2	3 days	no	2
F2-pre	3 days	yes	2
F3	3 days	no	3

TEM images were obtained on a Philips CM20 transmission electron microscope equipped with a LaB_6 electron gun. For each film, two TEM samples were prepared, one for cross section and one for planar view analysis: three 2 × 2 mm plates were prepared by cutting the sample at a fixed height of 1.5 cm from the base of the silica glass substrate. To produce the sample for cross section, two of the plates were glued together using epoxy in such a way that the film sides faced each other. The third plate was directly used for the preparation of the sample for planar view observations. A mechanical polishing procedure was carried out on all the samples to achieve a 20 μm thickness: on the direction parallel to the glass cut for the cross section sample, and on the direction perpendicular to the glass cut for the planar view sample. Final thinning to electron transparency was achieved by precision ion milling with two Ar guns at 5 keV (Gatan PIPS).

EXAFS measurements were performed on station 8.1 at the SRS (Daresbury Laboratory, UK). Data were collected at room temperature in fluorescence mode at the Fe (7112 eV) and Co (7709 eV) K-edges on the F3 sample treated at 350 °C in air and after the final reduction treatment at 800 °C in hydrogen flow. Data were also collected in transmission mode for some reference samples. A double Si(111) monochromator was used; higher order harmonic rejection was achieved by detuning the monochromator so that the transmitted flux was reduced by 50%. Data were analyzed using standard procedures;[33] more details can be found in refs 34−36.

Rutherford backscattering spectrometry (RBS) measurements were performed at the National Laboratory INFN at Legnaro, Italy, by using a $^4He^+$ beam at an energy of 2.2 MeV.

Magnetic measurements were performed on a Cryogenic S600 SQUID magnetometer. Data were corrected for the diamagnetic contribution of the silica substrate which was separately measured. Magnetic moments were normalized considering the metal amount as evaluated from RBS data. Zero field cooled (ZFC) and field cooled (FC) magnetizations were measured on the plane of the slide with an applied field of 5 mT.

3. Results and Discussion

3.1. Structure and Morphology. The XRD spectra of all the films treated at 350 °C present only the amorphous haloes due to SiO_2, and no crystalline peaks are detectable regardless of the aging of the sol. The XRD spectra of the films submitted to the final reduction treatment at 800 °C present different patterns depending on the sol aging; in particular, the films obtained from the sol aged up to 2 days only show the amorphous silica haloes, whereas the spectra of the films obtained from a sol aged for 3 days also show a broad crystalline peak centered at $2\theta = 44.6°$, as shown in Figure 1 where the angular region near this peak is shown for F1, F2, F2-pre, and F3 samples. This peak can be attributed to the main (110) reflection of either bcc FeCo alloy or pure bcc α-Fe.[37] Because of the broadening of the peak and the very similar lattice parameters of α-Fe and FeCo, XRD cannot give a conclusive answer on the formation of the alloy. The other peaks due to the bcc phase are barely detectable and therefore the angular range where they should appear is not shown. The peak intensity of the main peak is very low for the F1 sample and increases from F1 to F3 suggesting that the film thickness grows as a function of the number of dips, as expected. On the other hand, despite the same number of dips, the intensity of the peak for sample F2 is larger than for the F2-pre one, suggesting a smaller thickness in the latter sample.

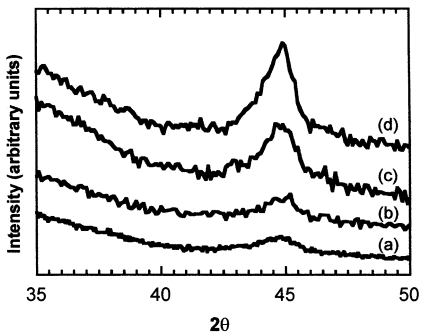

Figure 1. XRD spectra for the (a) F1, (b) F2-pre, (c) F2, and (d) F3 samples after the final thermal treatment at 800 °C in H_2 flow.

RBS spectra were analyzed using the RUMP program.[38] Because of the similar mass of Co and Fe atoms it is not possible to distinguish the Co and Fe profiles of the films. We obtained that the Fe + Co composition in all the films is almost uniform in depth. The metal content is slightly larger in the region of the film close to the substrate in the F2 sample, whereas in the F3 film the region near the surface has a larger metal content. From the calculation of the metal doses and assuming that all the Fe and Co are present in the metallic state, the maximum volumetric concentration of particles in the matrix is around 2.6%.

The cross section TEM analysis was used to evaluate the thickness, *t*, of the films and their homogeneity. The results clearly indicate that film thickness strongly depends on the experimental preparation conditions. For the F2-pre sample a uniform thickness $t = 90$ (±10) nm was measured (see Figure 2a). Uniform $t = 120$ (±10) nm was measured for the F2 sample (Figure 2b), but for the F3 sample (Figure 2c) a significant variation in thickness was observed — in particular, $t = 125$ (±10) nm on the right side, while $t = 80$ (±) 10 nm on the left side. It should be pointed out that the two sides correspond to portions of the films which are quite close to each other and therefore the F3 sample shows clear signs of thickness inhomogeneity. Furthermore, the F2 and F3 samples show the presence of a long nanoparticle chain which corresponds to the cross section image of a layer at the boundary with the silica glass substrate. This effect was not observed in the F2-pre sample which was obtained performing a pretreatment of the sub-

(33) Koningsberger, D. C.; Prins, R. *X-ray Absorption: Principles, Applications, Techniques of EXAFS, SEXAFS and XANES*; Wiley: New York, 1988.
(34) Corrias, A.; Mountjoy, G.; Piccaluga, G.; Solinas, S. *J. Phys. Chem. B* **1999**, *103*, 10081.
(35) Corrias, A.; Ennas, G.; Mountjoy, G.; Paschina, G. *Phys. Chem. Chem. Phys.* **2000**, *2*, 1045.
(36) Corrias, A.; Casula, M. F.; Ennas, G.; Marras, S.; Navarra, G.; Mountjoy, G. *J. Phys. Chem. B* **2003**, *107* (13), 3030−3039.
(37) PDF-2 File, JCPDS International Centre for Diffraction Data, 1601 Park Lane, Swarthmore, PA.
(38) Doolittle, L. R. *Nucl. Instr. Methods B.* **1985**, *9*, 334.

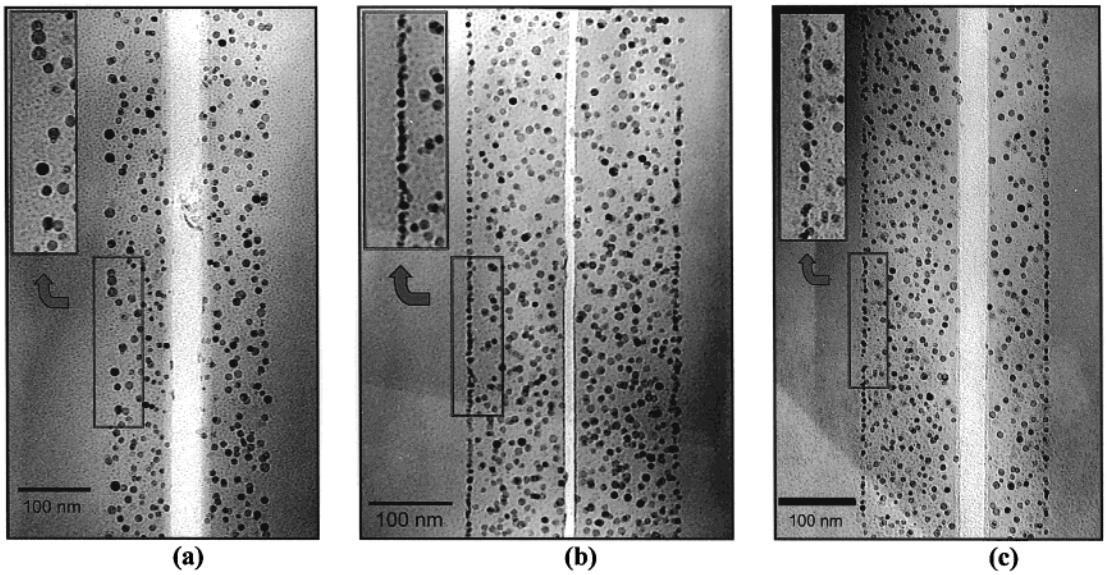

Figure 2. Cross-section TEM images for the (a) F2-pre, (b) F2, and (c) F3 samples after the final thermal treatment at 800 °C in H_2 flow. In the insets the detail of the boundary between the substrate and the film is shown.

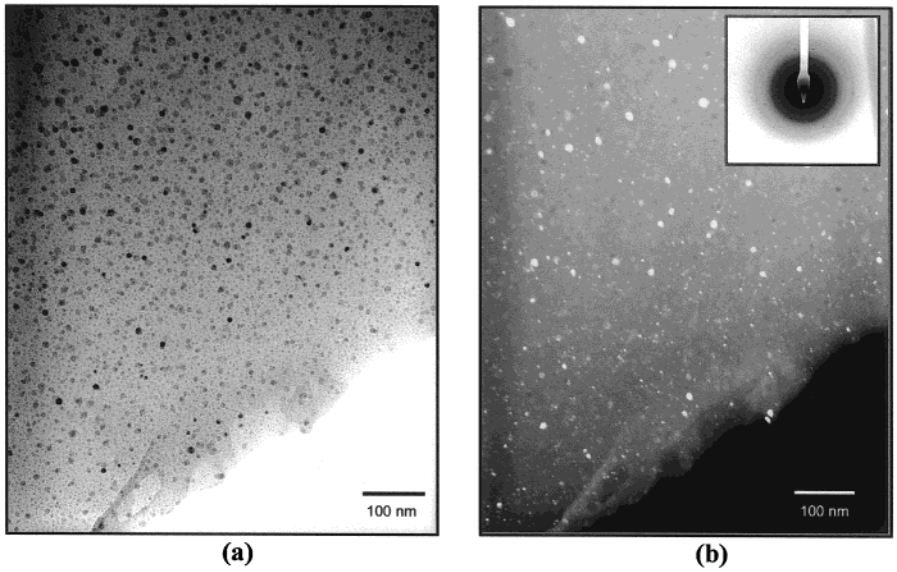

Figure 3. Planar view TEM images for the F2-pre sample: (a) bright field and (b) dark field. In the insert the diffraction pattern is shown.

strate with a mild alkaline solution. It is therefore likely that the formation of the layer of nanoparticles is strictly related to the surface characteristics of the silica glass substrate.

The planar view images of the F2, F2-pre, and F3 samples are all very similar; a typical example is shown in Figure 3. The nanoparticles have spherical shapes and they are well dispersed into the matrix. No layer of particles is observed in the planar view images of any sample. The nanoparticle size histograms for each sample were obtained using both cross section and planar view images. The particle size distributions were fitted to a log-normal distribution and gave average diameters of 8 ± 1, 9 ± 1, and 10 ± 1 nm with log-normal deviations of 0.15, 0.18, and 0.14 for F2, F2-pre, and F3, respectively.

All the electron diffraction images, collected with a camera length $L = 700$ mm, show a pattern typical of a bcc structure. The calculated lattice parameter matches that of bcc FeCo (2.86 Å), but, as already observed by XRD, the formation of the alloy cannot be certainly stated because the difference with the value of pure bcc Fe is within the experimental error.

The selectivity of the EXAFS spectroscopy was used to get a deeper insight on the structure of the nanoparticles by collecting data on the F3 sample treated at 350 °C in air and after the final treatment in H_2 flow at 800 °C.

The spectra at the Fe and Co K-edge of the film treated at 350 °C are compared in Figure 4A and B with those of $CoFe_2O_4$. Even if the spectra of the film are noisy, the position of the oscillations in the spectra of the film are consistent with the presence of very small particles (2−3 nm) of $CoFe_2O_4$ in the film. It should be pointed out that this phase was identified more accurately in a xerogel sample obtained starting from the same sol used for the film, as a consequence of the better quality of the EXAFS data accompanied by the likely

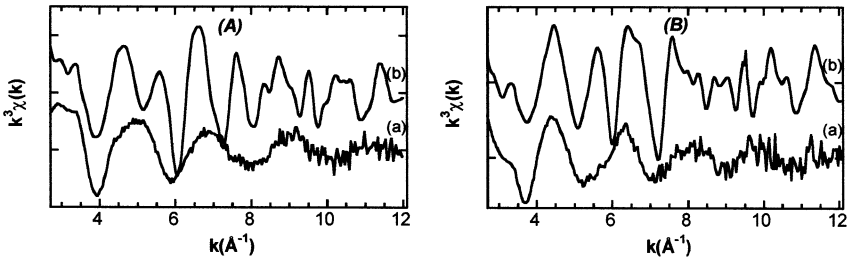

Figure 4. $k^3\chi(k)$ Spectra at the (A) Fe K-edge and (B) Co K-edge for the (a) F3 sample treated at 350 °C and (b) $CoFe_2O_4$.

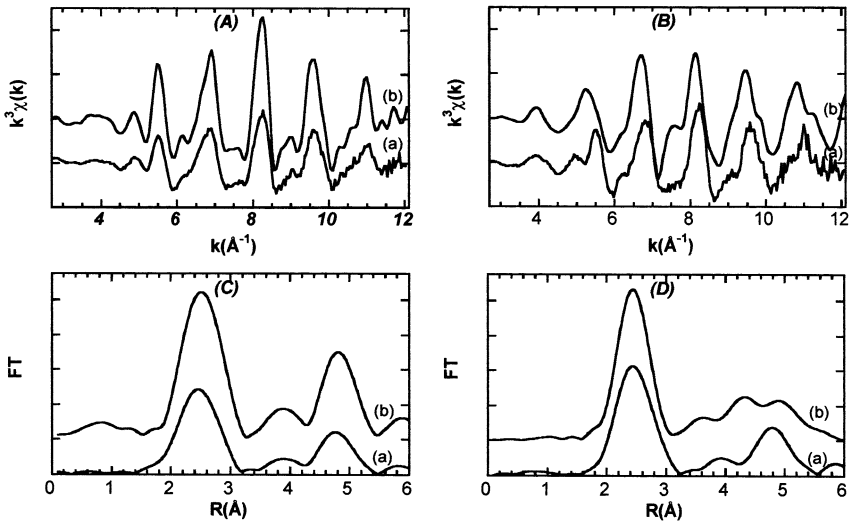

Figure 5. $k^3\chi(k)$ Spectra at the (A) Fe K-edge and (B) Co K-edge and Fourier transforms at the (C) Fe K-edge and (D) Co K-edge for the (a) F3 sample treated at 800 °C and (b) the reference metal foils.

presence of larger nanoparticles.[36] The indication of the presence of a highly dispersed phase on the film treated at 350 °C is in agreement with the XRD spectra where crystalline peaks were not detectable.

In Figure 5A and B the EXAFS spectra at the Fe and Co edge of the same film after the final reduction treatment at 800 °C are compared to those of bcc iron and fcc Co foils, respectively. The spectra of the film are noisier than those of the reference foils; however, oscillations are evident up to high *k* indicating that the nanoparticles in the film are larger than a few nanometers,[39] in agreement with the average crystallite size determined by TEM. The spectrum of the film at the Fe edge presents the same oscillations of the bcc Fe. On the other hand, the spectrum at the Co edge shows some significant differences with respect to fcc Co and is actually very similar to bcc Fe, indicating that a bcc FeCo alloy is formed. This can be seen even better by looking at the corresponding Fourier transforms (FT), which are reported in Figure 5C and D for the Fe and Co edge, respectively. The FTs of the film at both edges look very similar to each other and to bcc Fe, whereas that of fcc Co is definitely different. The selectivity of the EXAFS technique gives a clear and definite confirmation of the formation of bcc FeCo alloy nanoparticles which was not available from diffraction observations. A further confirmation was given by an EELS study on the same sample which showed the contemporary presence of the two metals in each nanoparticle.[40]

It should be pointed out that a detailed quantitative analysis of the same EXAFS data, reported elsewhere,[36] allows us to exclude that the Fe and Co atoms are present in forms other than nanocrystalline FeCo alloy apart from traces of impurities.

It is quite interesting to note that a significant fraction of iron in oxidized form and some unalloyed cobalt were detected on a xerogel sample obtained from the same sol.[30,36] The difference between the film and the xerogel sample was also confirmed by EELS spectroscopy[40] which evidenced the presence of an outer layer of oxide in the FeCo nanoparticles of the xerogel sample which is not present in the film. Even if textural data on the film samples are not available, it is likely that the films are denser than the xerogels so that the matrix protects the nanoparticles against oxidation. In accordance with this view EELS results pointed out that the nanoparticles in the films are closely surrounded by the matrix, but in the xerogel samples there is some free space between the nanoparticles and the matrix which can favor oxidation.[40]

3.2. Magnetic Properties. Considering the most striking difference evidenced by the structural and morphological characterization of the F1, F2, F2-pre, and F3 samples is the presence of a layer of particles at the boundary between the substrate and the film in the samples obtained using substrates not submitted to a pretreatment, the magnetic properties of the F2 and F2-pre films were investigated.

The field dependence of the magnetization recorded at 3 K for samples F2 and F2-pre is shown in Figure 6. In both cases a saturation is reached above ca. 20 kOe.

(39) Greegor, R. B.; Lytle, F. W. *J. Catalysis* **1980**, *63*, 476.
(40) Falqui, A.; Serin, V.; Calmels, L.; Snoeck, E.; Corrias, A.; Ennas, G. *J. Electron Microsc.* **2003**, *210*, 80−88.

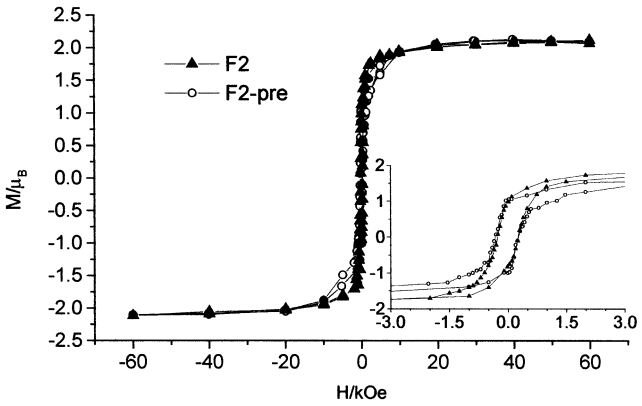

Figure 6. Field dependence of the magnetization recorded at 3 K for the samples F2 and F2-pre. In the inset the hysteresis loops in the ±3 kOe range are reported

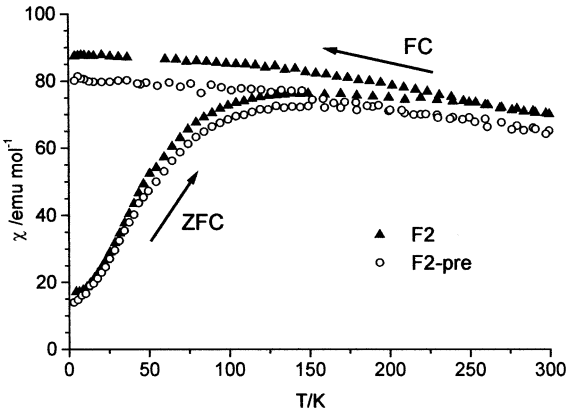

Figure 7. ZFC and FC susceptibilities of the F2 and F2-pre samples. All the curves were measured with an applied field of 5 mT.

The saturation magnetization per metal atom is 2.1 ± 0.2 μ_B for both samples, as expected for a bulk FeCo alloy. This confirms the effective formation of the nanocrystalline FeCo alloy and is a further indication that no crystalline phase other than the alloy is present, in agreement with the results obtained from EXAFS and EELS measurements.[36,40]

The hysteresis loops measured at room temperature show no coercivity, indicating that the samples are superparamagnetic. This is confirmed by the shape of the ZFC and FC static susceptibility curves reported in Figure 7. Below ca. 250 K the characteristic irreversibility due to the blocking−unblocking process of the particle magnetic moments is observed for all the samples. The maxima of the ZFC curves are broad as a consequence of the nanoparticles volume distribution. The temperatures corresponding to the maxima, T_{max}, are linked through a complex way to the mean blocking temperature of the samples that is related to the mean volume of the nanoparticles. The trend of the T_{max} of the ZFC curves (T_{max} equal to 140 K and 150 K for F2 and F2-pre films, respectively) is in agreement with mean diameters of the nanoparticles obtained by TEM analysis. Below the blocking temperature the hysteresis loops are open with similar coercive fields, which at 3 K are 260 Oe for F2 and 300 Oe for F2-pre sample (inset of Figure 6). The reduced remanent magnetization (M_r/M_S) values are 0.35 for F2 and 0.41 for F2-pre sample, respectively. The lower values of the coercive field and reduced remanent magnetizations obtained for the F2 sample with respect to those of the F2-pre sample could be ascribed to the stronger interparticle interactions, which are expected to decrease both the remanence and the coercivity.[41] In fact, as revealed by the TEM analysis, in the samples obtained using a substrate which is not pretreated with potassium hydroxide a uniform layer of FeCo nanoparticles in close contact is present at the boundary between the film and the substrate, where significant dipolar interactions may take place.

However, it should be pointed out that interparticle interactions are relevant in all FeCo−SiO_2 samples due to the large magnetic moment and the reduced anisotropy of the FeCo alloy. In agreement with this the ZFC susceptibilities are not strongly reduced above T_{max}, as expected from the Curie law, and the superparamagnetic susceptibility remains high at room temperature. This behavior makes the FeCo−SiO_2 system interesting for high-frequency applications.

It is interesting to compare the magnetic properties of the FeCo−SiO_2 films with those of FeCo−SiO_2 xerogel samples obtained from the same sol.[30] In particular, the xerogel samples present a lower saturation magnetization due to the presence of an oxide layer on the surface of the nanoparticles and the FeCo nanoparticles are still blocked at room temperature while at the same temperature all the FeCo nanoparticles in the film samples are in the superparamagnetic state. Because the mean diameter of the FeCo nanoparticles is quite similar in the xerogel and film samples, it is likely that the differences are due to the presence/absence of an oxide layer contamination which is known to play an important role in the average magnetic behavior.[9,42]

From the mean diameter obtained by TEM investigation and assuming that on the time scale of our experiment the mean magnetic anisotropy constant is given by $\langle K\rangle = 25k_BT_{max}/\langle V\rangle$, where $\langle V\rangle$ is the mean particle volume, a rough determination of $\langle K\rangle$ was attempted. For all the films a $\langle K\rangle$ value of the order of 10^5 J/m^3 was estimated. This value is larger than the one of FeCo bulk alloy, as expected for the nanoparticles where the surface and shape contribute to increase the total anisotropy.[3]

4. Conclusion

The sol−gel method was used with success to prepare FeCo−SiO_2 nanocomposite films on silica glass substrates. Spherical FeCo alloy nanoparticles with average dimensions around 10 nm are obtained in all the samples. Particles are well dispersed in the silica matrix and show superparamagnetic behavior.

EXAFS and magnetic data point out that no trace of unalloyed metal is present, indicating that the preparation is successful. Moreover, the FeCo alloy nanoparticles are practically pure and no significant oxidation is observed. This is probably due to the low porosity of the sol−gel SiO_2 matrix which protects the nanoparticles from oxidation.

(41) El-Hilo, M.; Chantrell, R. W.; O'Grady, K. *J. Appl. Phys.* **1998**, *84*, 5114.
(42) Gangopadhyay, S.; Hadjipanayis, G. C.; Shah, S. I.; Sorensen, C. M.; Klabunde, K. J.; Papaefthymiou, V.; Kostikas, A. *J. Appl. Phys.* **1991**, *70*, 5888.

The experimental conditions influence the thickness and homogeneity of the films. In particular, the multiple dipping technique can be used to obtain films of about 100-nm thickness; however, the films tend to become inhomogeneous after the third dip. When the glass substrate is just cleaned prior to dipping, a layer of nanoparticles is formed at the interface between the substrate and the film. This layer is not formed if the substrate is first submitted to a treatment with a mild alkaline solution. It is well-know that alkaline solutions can break Si−O−Si bridging bonds forming Si−OH groups at the surface of the glass modifying the wettability of the substrate since the surface is hydrophilic. Moreover, the treatment can alter the roughness of the substrate surface and it is likely that these aspects play an important role in avoiding the formation of the layer of nanoparticles. Further studies are in progress to explain this behavior in more detail.

The difference in thickness between the F2 and F2-pre samples is also likely to depend on the different surface behavior of the substrate.

The samples are in the superparamagnetic state at room temperature and the magnetic properties of the samples are affected by the pretreatment of the substrate as a consequence of different interparticle interactions which influence both the remanence and the coercivity.

Acknowledgment. We acknowledge Ministero dell'Istruzione, dell'Università e della Ricerca (MIUR, Prin 2001038849 004) for financial support, and the European Community Access of Research Infrastructure action of the Improving Human Potential Program for accessing the SRS Synchrotron. A. Falqui has been supported by the European Community Improving Human Potential Program under contract HPMF-CT-2000-01007.

CM0217755